European Society of Computational Methods
in Sciences and Engineering (ESCMSE)

Journal of Numerical Analysis,
Industrial and Applied Mathematics
(JNAIAM)
vo19. , no. 1-2, 2026, pp. 57-69
ISSN 1790–8140

Assessment of Hull Surface Roughness Effects on KVLCC2 Ship Performance Using CFD and Katsui Correlation

Z. Ali and G. Bognár[1]

Institute of Machine and Product Design,
Faculty of Mechanical Engineering and Informatics,
University of Miskolc,
3515-Egyetemváros, Miskolc, Hungary

Abstract: Hull surface roughness, resulting from fouling or coating degradation, significantly increases hydrodynamic resistance, leading to higher fuel consumption and greenhouse gas emissions. This study investigates the impact of uniform full-hull roughness on the hydrodynamic performance of the KVLCC2 tanker through full-scale Computational Fluid Dynamics (CFD) simulations, complemented by predictions from the empirical Katsui Roughness Correlation. The analysis covers design and slow operating speeds, with roughness heights ranging from 0 to 5000 μm. CFD results quantify the increase in total resistance, effective power, and fuel demand, revealing frictional resistance as the dominant contributor at low Froude numbers. Comparisons with Katsui's predictions show consistent underestimation of resistance and power penalties, with discrepancies exceeding 50% for severe roughness. These findings indicate that sole reliance on Katsui may lead to significant underprediction of operational costs. Integrating CFD with empirical methods provides a more robust basis for performance assessment, supporting compliance with energy-efficiency regulations such as EEDI and SEEMP.

Keywords: Hull roughness, CFD, Katsui correlation, KVLCC2, frictional resistance, effective power, fuel consumption.

Mathematics Subject Classification: 76D07, 76M25, 65N30

PACS: 47.11.-j, 47.85.Dh, 47.55.-t

1. Introduction

Based on the shipping industry's perspective, constant pursuit of fuel optimization and pollution reduction has increased the demand for mathematically accurate predictive models of hydrodynamic resistance under practical operating conditions. Surface degradation phenomena like fouling and roughness, which function as boundary-layer turbulence that alter near-wall flow behavior and increase energy losses, have a significant impact on hull frictional resistance, which can dominate the total resistance at low and moderate Froude numbers and also effect the propeller performance, exacerbating energy losses if not managed appropriately [23]. Numerical evaluations based on CFD provide comprehensive insights into the relationship between surface roughness and ship resistance, guiding solutions to increase efficiency and lower emissions. The necessity for thorough information on the impact of roughness on different antifouling coatings and fouling types was emphasized by the ITTC (2011). These influences have been investigated for various vessel types in several studies, including studies by Schultz [2], Demirel et al. [3], Song et al. [4], Seok et al. (2020) [5], and Amiruddin et al. [15], while the ITTC (2011) has emphasized the necessity of improved predictive capability for roughness-induced resistance variations.

From a mathematical standpoint, the underlying problem can be defined as the numerical approximation of a coupled nonlinear system of partial differential equations, which includes the Reynolds-Averaged Navier–Stokes equations closed by the nonlinear k–ω SST turbulence model, set up on a domain where wall roughness effects are represented by boundary-induced parameter turbulence. The presence of surface roughness modifies the near-wall asymptotic structure of the solution, thereby affecting the regularity of the velocity field, the behaviour of the wall shear stress operator, and the stability properties of the discrete system. Consequently, the problem belongs to the category of nonlinear, multiscale, and boundary-sensitive PDE systems, where the position of the computed solution is largely dependent on numerical discretization, turbulence closure, and mesh resolution approach.

By analyzing the relationship between discretized PDE-based solutions and reduced-order simulation through a systematic comparison between high-quality CFD solutions and the Katsui roughness correlation, the current study advances Numerical Analysis and Applied Mathematics [12], [13]. This comparison can be interpreted as a numerical consistency study between a first-principles discretization of a nonlinear PDE system and an empirical algebraic closure model, highlighting the limitations of low-dimensional approximations in capturing nonlinear boundary-layer amplification effects in full-scale regimes. Therefore, this work focuses on discretization accuracy, convergence behaviour under mesh refinement, and model-form uncertainty in turbulence-affected boundary value problems.

2. Fluid flow model description

This study employs Computational Fluid Dynamics (CFD) to numerically simulate the Navier-Stokes equation and conservation of mass equation for incompressible Newtonian fluids [25]. ANSYS 15 serves as the CFD solver. The turbulence modelling uses the k-ω SST (Shear Stress Transport) model, a hybrid of the k-ω and k-ε turbulence models widely applied in recent CFD analyses for complex flow predictions such as vortex–induced structures and enhanced transport phenomena [24]. The k-ω SST model is commonly accepted for external marine flows as it balances near-wall accuracy with free-stream robustness [22]. This technique provides precise predictions of turbulent behavior, including governing equations for turbulent kinetic energy (k) and specific dissipation rate (ω) [6-10]:

$$k-\ equation\text{:}\ \frac{\partial \mathrm{k}}{\partial \mathrm{t}}+\mathrm{u_j}\frac{\partial \mathrm{k}}{\partial \mathrm{x_j}}=\mathrm{P_k}-\beta^*\mathrm{k}\omega+\frac{\partial}{\partial \mathrm{x_j}}\left[(\nu+\sigma_{\mathrm{k}}\nu_{\mathrm{T}})\frac{\partial \mathrm{k}}{\partial \mathrm{x_j}}\right], \tag{1}$$

$$\omega-equation\text{:}\ \frac{\partial \omega}{\partial \mathrm{t}}+\mathrm{u_j}\frac{\partial \omega}{\partial \mathrm{x_j}}=\alpha \mathrm{S}^2-\beta\omega^2+\frac{\partial}{\partial \mathrm{x_j}}\left[(\nu+\sigma_\omega\nu_{\mathrm{T}})\frac{\partial \omega}{\partial \mathrm{x_j}}\right]+2(1-\mathrm{F_1})\sigma_{\omega 2}\frac{1}{\omega}\frac{\partial \mathrm{k}}{\partial \mathrm{x_i}}\frac{\partial \omega}{\partial \mathrm{x_i}}, \tag{2}$$

$$\text{Eddy viscosity} - \text{equation: } \mu_{\mathrm{t}}=\frac{\rho\alpha_1 \mathrm{k}}{\max(\alpha_1\omega, \mathrm{SF_2})},\quad \mathrm{S}=\frac{\partial \mathrm{u}}{\partial \mathrm{y}}, \tag{3}$$

$$\mathrm{F_1}=\tanh\left\{\left\{\min\left[\max\left(\frac{\sqrt{\mathrm{k}}}{\beta^*\omega \mathrm{y}},\frac{500\nu}{\mathrm{y}^2\omega}\right),\frac{4\sigma_{\omega 2}\mathrm{k}}{\mathrm{CD_{k\omega}}\mathrm{y}^2}\right]\right\}^4\right\},\ \mathrm{F_2}=\tanh\left[\left[\max\left(\frac{\sqrt{\mathrm{k}}}{\beta^*\omega \mathrm{y}},\frac{500\nu}{\mathrm{y}^2\omega}\right)\right]^2\right],$$

$$\mathrm{P_k}=\min\left(\tau_{\mathrm{ij}}\frac{\partial \mathrm{u_i}}{\partial \mathrm{x_j}},10\beta^* CD_{\mathrm{k}\omega}\right), CD_{\mathrm{k}\omega}=\max\left(2\rho\sigma_{\omega 2}\frac{1}{\omega}\frac{\partial \mathrm{k}}{\partial \mathrm{x_i}}\frac{\partial \omega}{\partial \mathrm{x_i}},10^{-10}\right),$$

$$\tau_{\mathrm{ij}}=2\ \mu_t S_{ij}-\frac{2}{3}\rho k\delta_{ij}, \tag{4}$$

where, $\mathrm{u_i}, \mathrm{u_j}$ are the velocity components in the Cartesian directions $\mathrm{x_i}, \mathrm{x_j}$, respectively; k is the turbulent kinetic energy; ω is the specific dissipation rate; ν is the kinematic viscosity of the fluid; $\nu_{\mathrm{T}}, \mu_{\mathrm{T}}$ are the turbulent kinematic and dynamic eddy viscosities, respectively; ρ is the fluid density; $\mathrm{P_k}$ represents the production term of turbulent kinetic energy; S is the magnitude of the strain-rate tensor; τ_{ij} stress tensor (dynamic quantity); δ_{ij} is the Kronecker delta function, and S_{ij} is the mean strain-rate tensor (kinematic quantity) defined as $S_{ij}=\frac{1}{2}\left(\frac{\partial \mathrm{u_i}}{\partial \mathrm{x_j}}+\frac{\partial \mathrm{u_j}}{\partial \mathrm{x_i}}\right)$.

Furthermore, $\mathrm{F_1}, \mathrm{F_2}$ are blending functions used in the SST model to combine the near-wall formulation k-ω with the far-field k-ε behavior; $CD_{\mathrm{k}\omega}$ is the positive cross-diffusion term; y denotes the normal distance from the wall surface and $\alpha_{1,2}, \beta^*, \beta_{1,2}, \sigma_{k1,2}, \sigma_{\omega 1,2}$ are empirical model constants.

The turbulence model switches between the two modes using a blending function. The model parameters are provided in Table 1.

Table 1: Configurations of the models considered

β^*	α_1	β_1	σ_{k1}	σ_{k2}	$\sigma_{\omega 1}$	α_2	β_2	$\sigma_{\omega 2}$
0.09	0.555	0.075	0.85	1	0.5	0.44	0.828	0.856

2.1. Wall Roughness Boundary Condition

The hull surface roughness was modeled using a rough-wall boundary condition implemented within the ANSYS Fluent wall-function framework based on the equivalent sand-grain roughness approach. The near-wall velocity profile follows the logarithmic law of the wall [27]

$$U^{+}(y^{+}) = \frac{1}{k_{const}} \ln y^{+} + B\,;\ 5 \le y^{+} \le 30. \tag{5}$$

For rough surfaces, the velocity profile is modified through a roughness function

$$U^{+}(y^{+}) = \frac{1}{k_{const}} \ln y^{+} + B - \Delta U^{+}(k_s), \tag{6}$$

where B is the integration constant of the smooth-wall log-law, while $k_{const} = 0.41$ is the von Kármán constant [26]; (k_s) is the equivalent sand-grain roughness height and ΔU^{+} is the roughness function representing the downward shift in the logarithmic velocity profile caused by surface irregularities.

3. Geometrical dimensions and boundary conditions

The KVLCC2 ship tanker model was chosen due to its extensive experimental data availability, making it a reliable option for our study. Its dimensions are detailed in reference [11]. The investigation was conducted at Froude number F_r =0.142, allowing us to neglect wave resistance and consider density (998.2 kgm^{-3}), viscosity (0.001003 Pas), and the ratio of specific heat (1.4).

In CFD applications, ensuring numerical equations and model quality and accuracy is vital. Our results were thoroughly evaluated and compared with experimental data, with Schultz's study [2] providing a trusted benchmark for calculating resistance coefficients with surface roughness.

The plate used in the experiment is 1.52 m in length, 590 mm in height, and 3.2 mm in thickness, with smoothed edges (semi-circular with a 1.6 mm diameter) identical to Schultz's study [2].

4. Mesh Independence and Grid Convergence Index (GCI) Analysis

To ensure the mathematical reliability and numerical consistency of the CFD solution, a systematic grid independence study was performed using four refined meshes, ranging from 770,659 to 1,367,894 cells. The total resistance coefficient C_T was selected as the primary monitored variable. A representative roughness height of $(d = 5000\,\mu m)$ was chosen for the convergence analysis due to its highest sensitivity to surface roughness effects.

The mesh configurations and their associated numerical results are presented in Table 2 [27]).

Table 2: Total drag coefficient C_T for different mesh configurations

$d(\mu m)$	C_T (1367894)	C_T (1187640)	C_T (950891)	C_T (770659)
500	0.0054502	0.0054504	0.0055009	0.0056101
1000	0.0069571	0.0069575	0.0072241	0.0074922
2000	0.0073160	0.0073167	0.0073764	0.0074585
3000	0.0078519	0.0078524	0.0078892	0.0080092
4000	0.0082589	0.0082590	0.0084982	0.0084509
5000	0.0085963	0.0085967	0.0086676	0.0086290

With increasing mesh refinement, a monotonic convergence tendency is observed, indicating that the numerical solution approaches an asymptotic value. To quantify discretization uncertainty, the Grid Convergence Index (GCI) methodology based on Richardson extrapolation was applied. The formulation of GCI is provided by [28], [29]:

$$GCI_{12} = \frac{1.25|\varepsilon_{12}|}{r^{p}-1} \times 100\%, \tag{7}$$

$$\varepsilon_{12} = \frac{f_1 - f_2}{f_1}, \tag{8}$$

where, r is the refinement ratio between successive grids, and p is the order of accuracy of the numerical scheme.

The Richardson extrapolation for the asymptotic solution is formulated as:

$$f_{ext} = f_1 + \frac{f_1 - f_2}{r^p - 1}. \tag{9}$$

For the present study, the refinement ratio is approximated as $r \approx 1.25$, while a second-order spatial discretization scheme $p = 2$ is assumed to be consistent with the numerical methods implemented in the CFD solver.

Considering the finest and medium meshes, the relative error is computed as:

$$\varepsilon_{12} = \frac{\left|C_T^{fine} - C_T^{medium}\right|}{C_T^{fine}} = 4.65 \times 10^{-5}, \tag{10}$$

$$GCI_{12} = \frac{1.25 \times 4.65 \times 10^{-5}}{1.25^2 - 1} \approx 1.03 \times 10^{-4} \approx 0.01\%. \tag{11}$$

The obtained GCI confirms that the solution is within the asymptotic convergence range and that the discretization error is negligible. Accordingly, the mesh with 1,187,640 cells is adopted as the reference grid. Since a second-order spatial discretization scheme is employed $p = 2$ and the observed convergence behavior confirms monotonic refinement, the discretization error follows the asymptotic trend:

$$\varepsilon = \mathcal{O}(\Delta x^2). \tag{12}$$

This indicates that numerical uncertainty decreases quadratically with mesh refinement, consistent with second-order accuracy.

5. Numerical Implementation and results

A structured grid comprising 482,576 nodes was generated in ICEM for the symmetric ship model, with cells oriented normal to the hull surface to resolve the viscous flow field accurately. Higher mesh density was assigned to the bow, stern, and run regions to improve local flow prediction. Similarly, a structured grid for the plate was created with 1,187,640 nodes and a growth rate of 1.2.
Numerical simulations employed the Finite Element Method (FEM) in ANSYS, using a coupled Pressure-Based solver with a SIMPLE–PISO scheme to resolve the continuity and momentum equations. Spatial discretization applied least-squares cell-based gradients, second order upwind for pressure and momentum, and first-order upwind for turbulent kinetic energy and specific dissipation rate. Steady-state conditions were assumed, with Hybrid initialization of flow variables.

5.1. Influence of the (full/divided) hull roughness on the ship's total resistance

Table 3 summarises the computed resistance coefficients for a ship operating at a Froude number of 0.142 (v_{ship} = 15.5knots), considering uniform hull roughness heights (d) between 0.5 mm and 5 mm. The clean hull baseline coefficient is 0.00411. Results indicate a pronounced increase in total resistance with rising roughness, exceeding 100% for $d = 5$ mm. This confirms that large-scale surface roughness can significantly impair hydrodynamic performance.

Table 3: Total resistance coefficients at different roughness heights with $Fr = 0.142$.

$d(\mu m)$	$C_{T,CFD}$
500	0.0054504
1000	0.0069575
2000	0.0073167
3000	0.0078524
4000	0.0082590
5000	0.0085967

Localized flow disturbances have been demonstrated to be generated by zonal roughness distribution [17]; therefore, the carrier ship's hull was divided into three sections: Bow, Center, and Stern. Numerical simulations evaluated the impact of roughness on drag resistance in each section, considering various roughness heights. Table 4 compares drag coefficients between the roughened hull and a clean hull (without roughness). Results show a significant increase in drag coefficient, exceeding 103%, with 7.5 mm roughness in the Center area. The Stern area experienced a 26.884% increase, and the Bow area saw a 13.340% rise in drag coefficient for the same roughness height (see Fig.1).

Table 4: The percentage of the increase in the resistance modulus at different heights of roughness in comparison with the clean body condition

$d(\mu m)$	$\Delta C_d\%$ (Bow)	$\Delta C_d\%$ $(Center)$	$\Delta C_d\%$ $(Stern)$	$\Delta C_d\%$ $(Full\ body)$
0	0	0	0	0
85	0.792	2.42	0.69	3.084
150	1.456	7.053	1.712	9.378
200	2.121	10.759	2.581	14.387
500	5.111	29.568	7.487	39.713
750	6.670	40.173	10.554	53.973
1000	7.743	47.968	12.777	64.370
5000	12.484	90.391	23.945	120.163
7500	13.340	103.168	26.884	137.158
10000	13.723	113.135	29.056	150

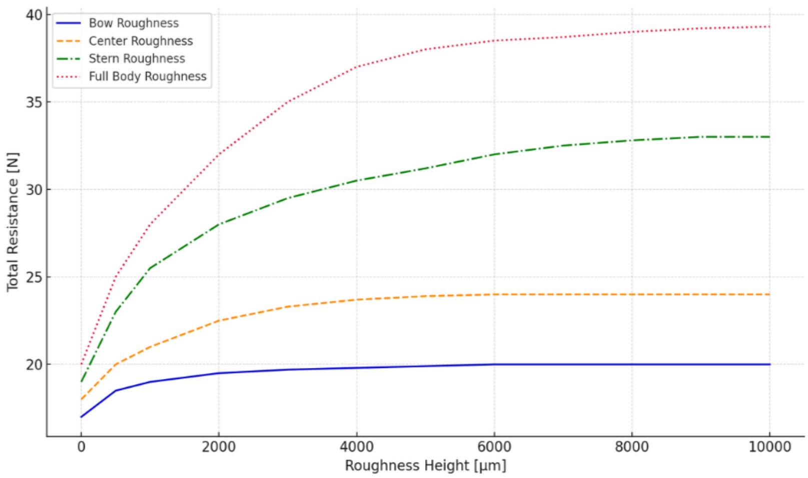

Figure 1: Drag coefficient C_d according to roughness height.

5.2. Influence of surface roughness on the components of pressure and friction forces

In ship hydrodynamics, total resistance primarily comprises pressure and frictional components. At low Froude numbers, frictional resistance can contribute up to 80% of the total. Therefore, isolating the influence of hull roughness on each component is essential [15]. Figure 2 presents the variation in total resistance for different roughness distributions, while Figure 3 compares the relative contributions of pressure and frictional forces across the hull. Results show that surface roughness markedly increases frictional resistance, whereas its effect on pressure resistance is minimal. This distinction is critical for performance optimization, especially under conditions where friction dominates total resistance. Hakim et al. [18] reached comparable conclusions, demonstrating that inhomogeneous surface roughness patterns substantially contribute to non-uniform drag distribution across planning hulls.

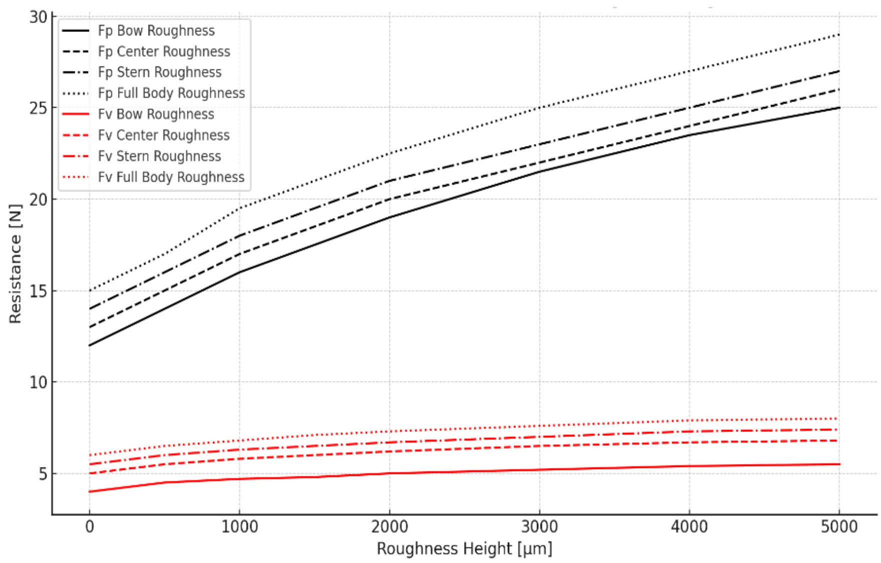

Figure 2: The variations in the ship's total resistance occur as the roughness of different hull sections changes.

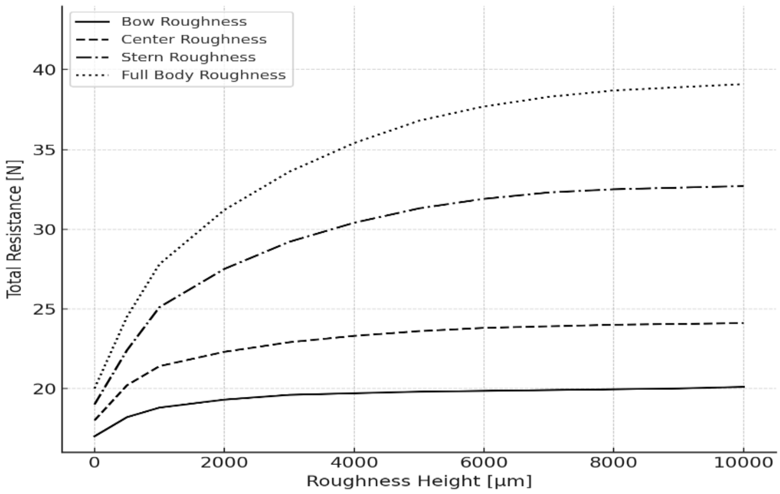

Figure 3: Pressure F_P and frictional resistance F_V exhibit variations with different roughness heights across each hull section.

5.3. Influence of Hull Roughness on Frictional and Residual Resistance Ratios

The effect of hull surface condition on resistance components over a range of Froude numbers is further quantified in Figures 4 and 5. The frictional to total resistance ratios for smooth and rough hull scenarios are shown in Figure 4, with the rough-hull configuration showing consistently higher ratios, especially at lower speeds. The residual resistance coefficient variation is shown in Figure 5, which indicates a noticeable increase for the rough hull with increasing speed. These results confirm that the main effect of hull roughness is to increase frictional resistance, which in turn increases residual resistance. The results validate that hull roughness primarily elevates frictional resistance, subsequently augmenting residual resistance due to hydrodynamic interactions, with trends significantly affected by operating speed [20].

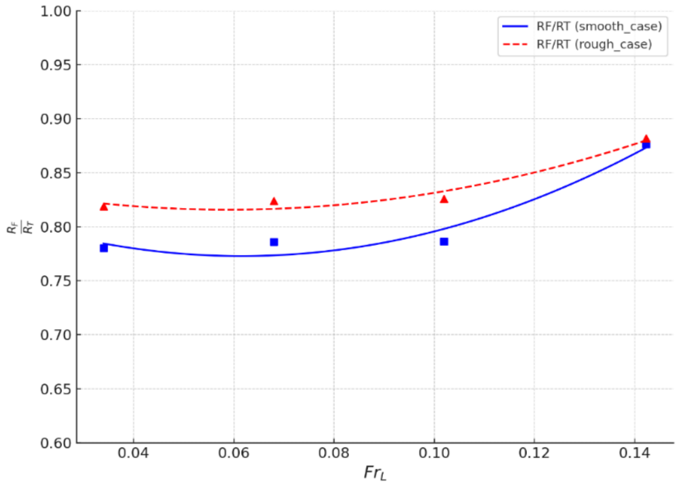

Figure 4: Ratio of frictional to total resistance (R_F/R_T) for smooth and rough hulls at different Fr_L.

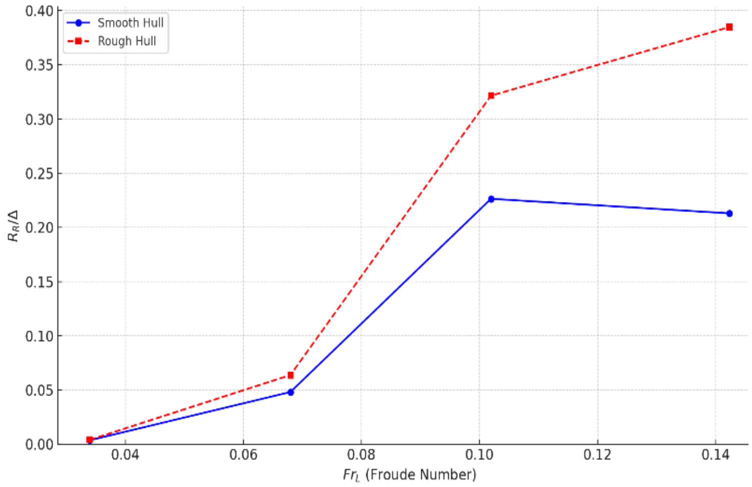

Figure 5: Residual resistance (R_R/Δ) for smooth and rough hulls across Froude numbers.

5.4. Katsui Roughness Correlation

The Katsui line is an empirical correlation developed to estimate the additional frictional resistance caused by hull surface roughness. Originally proposed by Katsui (1984) and later incorporated into ITTC recommendations, the correlation has been widely applied to scale model test results to full-scale conditions.
The Katsui roughness allowance has been documented in multiple functional forms in the literature. A widely cited empirical formulation is given as [12], [13]:

$$\Delta C_F = \left(105\left(\frac{k_s}{L_{wl}}\right)^{1/3} - 0.64\right) \times 10^{-3}. \tag{13}$$

In the present study, a simplified Katsui-type formulation in power-law form for empirical comparison with CFD results [12], [13].

$$\Delta C_F = 0.044\left(\frac{k_s}{L_{wl}}\right)^{0.31}, \tag{14}$$

where, ΔC_F is the roughness allowance, k_s is the equivalent roughness height (m), and L_{wl} is the ship's length on the waterline (m). This method is intended to correct the ITTC-1957 friction line [12], [13] by adding a roughness allowance to obtain the total resistance coefficient C_T.

The empirical nature of the Katsui correlation makes it computationally inexpensive and straightforward to apply. However, its accuracy for large, full-bodied ships such as KVLCCs, operating at low Froude numbers, has not been extensively validated. This study, therefore, compares Katsui's predictions with the present CFD results for the KVLCC2 to assess its reliability for such hull forms.

For the present study, in nominal velocity 15.5 knots, the full-scale parameters of the KVLCC2 were considered, $L_{wl} = 320$m, wetted surface area for the full-scale KVLCC2 is 27.194 m^2 [11].

The smooth-hull ITTC-1957 friction coefficient was first calculated as:

$$C_F^{smooth} = \frac{0.075}{(log_{10}Re-2)^2}. \tag{15}$$

For each roughness height k_s, ΔC_F were computed using the Katsui formula and added to C_F^{smooth}. The total resistance coefficient is then obtained as:

$$C_T = (C_F^{smooth} + \Delta C_F) + C_P, \tag{16}$$

$$R_T = \frac{1}{2}\rho S C_T V^2. \tag{17}$$

5.5. Comparison Between Katsui Predictions and CFD Results

Table 5 compares total resistance coefficients from CFD simulations and Katsui correlation estimates for KVLCC2 at nominal service speed (Fr = 0.142) with uniform hull roughness. Katsui consistently underpredicts total resistance, with deviations ranging from 47% for the smooth hull to −58% at the maximum roughness (5 mm). Figure 6 displays the comparison with a secondary axis showing the percentage difference. These findings suggest that for large, full-bodied hull forms operating at low Froude numbers, especially when roughness effects are substantial, the Katsui correlation may not be accurate.

Table 5: CFD and Katsui total resistance coefficients for KVLCC2 at Fr = 0.142 with varying hull roughness

$d(\mu m)$	$C_{T,CFD}$	$C_{T,Katsui}$	$Difference$ %
0	0.00411	0.00216	47.27
500	0.00545	0.00286	47.44
1000	0.00695	0.00303	56.42
2000	0.00731	0.00323	55.73
3000	0.00785	0.00338	56.92
4000	0.00825	0.00349	57.67
5000	0.00859	0.00359	58.23

These results demonstrate that the Katsui correlation consistently underpredicts the total resistance coefficient compared to the CFD results, with differences ranging from approximately −47% for the smooth hull to −58% for the highest roughness height.

Figure 6 compares CFD and Katsui predictions of the total resistance coefficient for KVLCC2 at nominal speed (1.047 m/s), with a secondary axis showing the relative difference (%) between the two. Lopes et al. [19] found analogous findings concerning the constraints of empirical predictions and the benefits of full-scale CFD resistance estimations, thereby strengthening the dependability of numerical approaches for evaluating roughness effects under operational settings.

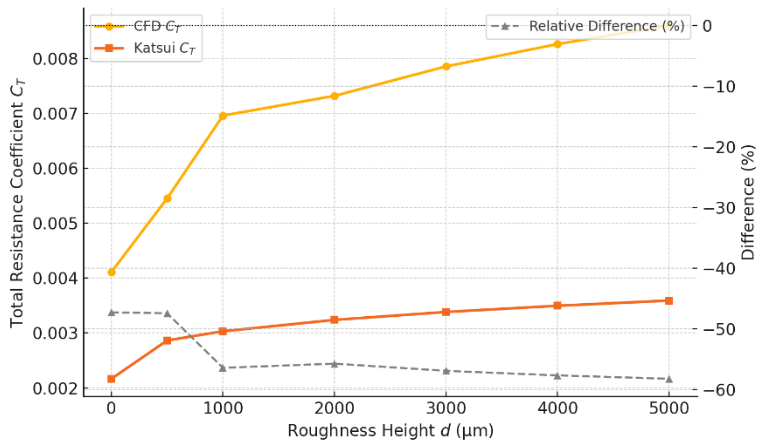

Figure 6: CFD vs. Katsui total resistance coefficients for KVLCC2 at nominal speed, with relative difference (%).

5.6. Exploring the Interplay Between Resistance and Ship Performance

The influence of hull roughness on fuel consumption was evaluated by quantifying the resulting increase in total resistance for the KVLCC2. Higher resistance directly translates into greater effective power demand and the energy required to overcome hydrodynamic forces and maintain vessel speed. The concept of effective power (P_E) is directly linked to both the total resistance (R_T) and the ship's operating velocity (v_{ship}).

$$P_E(kW) = R_T(N) \times v_{ship}(knot), \tag{18}$$

$$R_T = \frac{1}{2} \times \rho \times S \times C_T \times v_{ship}^2, \tag{19}$$

where ρ is the density of water, S is the wetted surface area, and C_T is the total resistance coefficient. Therefore, we can rewrite P_E as follows:

$$P_E = \frac{1}{2} \times \rho \times S \times C_T \times v_{ship}^3. \tag{20}$$

CFD simulations accurately anticipated the full-scale KVLCC2's overall drag coefficients. Table 6 shows the increase in effective power and total resistance for various roughness heights compared to the smooth hull at design speed (15.5 knots) and moderate operational speeds (3.7, 7.4, and 11.1 knots). Effective power increases by 91% at 15.5 knots and 96% at 7.4 knots at a roughness height of 5000 μm (Table 6), highlighting the severe performance penalty associated with extreme hull roughness. Even modest fouling might result in severe speed disadvantages due to hull roughness [21].

Table 6: Computed P_E values for the KVLCC2 full-scale model at different velocities $3.7, 7.4, 11.1$ and 15.5 $knots$.

d (μm)	$P_E(kW)$			
	3.7 $knots$	7.4 $knots$	11.1 $knots$	15.5 $knots$
0	0.1382	3.7416	26.4921	69.3514
500	0.1444	4.4624	33.5824	84.0482
1000	0.1590	5.2155	39.6071	98.9275
1500	0.1734	5.7615	43.4535	107.2886
2000	0.1862	6.1661	46.0105	112.8276
3000	0.2067	6.7000	49.4417	121.0881
4000	0.2216	7.0556	52.0124	127.3599
5000	0.2324	7.3437	53.9688	132.5659

5.7. Added Power Estimation Using Katsui Roughness Allowance

The Katsui correlation can estimate the additional effective power (ΔPE) needed to overcome full-scale hull roughness in addition to predicting total resistance coefficients:

$$\Delta PE = PE_{rough} - PE_{smooth} \tag{21}$$

Table 7 presents Katsui-based estimates for KVLCC2 at design speed across various roughness heights. At 5000 µm, the method predicts a 10.14 MW increase in effective power relative to the smooth hull. Figure 7 shows both the estimated effective power and ΔPE, illustrating a clear upward trend with increasing roughness and highlighting the associated energy penalty.

Table 7: Katsui-estimated effective and additional power for KVLCC2 at design speed under varying hull roughness

$d(\mu m)$	$C_{T,Katsui}$	R_T(N)	$PE\ (Kw)$	$\Delta PE\ (Kw)$
0	0.002167	1.92×10^6	15,284	—
500	0.002865	2.54×10^6	20,183	4,899
1000	0.003032	2.69×10^6	21,389	6,105
2000	0.003239	2.87×10^6	22,843	7,559
3000	0.003383	3.00×10^6	23,946	8,662
4000	0.003496	3.10×10^6	24,762	9,478
5000	0.003591	3.18×10^6	25,425	10,141

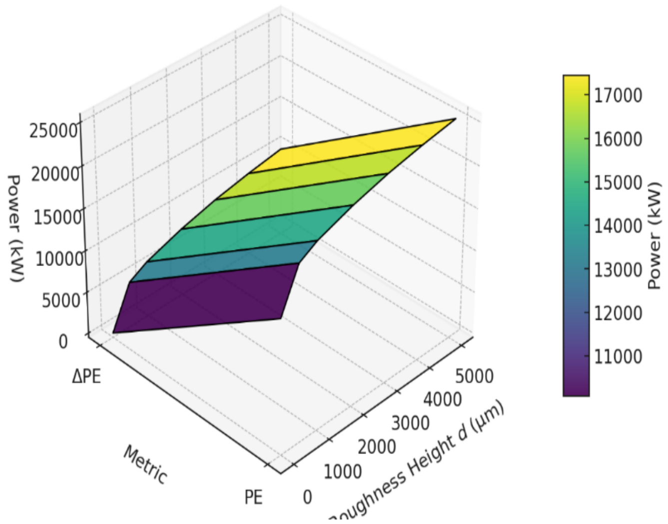

Figure 7: Katsui-predicted effective power and additional power (ΔPE) for KVLCC2 at design speed.

Katsui estimates an extra 4.9 MW demand for moderate fouling (500 µm); however, this study's CFD results show significantly higher penalties. This implies that, despite its computational efficiency, Katsui understates the practical effects of large, full-bodied hulls, especially in energy efficiency. A more reliable foundation for operational cost forecasting and EEDI/SEEMP compliance is provided by a combined Katsui–CFD approach. [12], [13], and [14].

6. Conclusion

The full-scale CFD simulations for KVLCC2 reveal that hull roughness significantly increases frictional resistance, especially at low operating speeds, while pressure resistance remains largely unaffected. Severe fouling can raise effective power demand by up to 96%, underscoring the operational impact. Katsui correlation consistently underestimates resistance and power penalties by 47–58%, making it insufficient for accurate performance forecasting. Integrating CFD with empirical methods offers a more reliable foundation for fuel budgeting and compliance with energy-efficiency regulations. Future studies may explore hybrid modelling approaches or extend analysis to other hull forms and fouling conditions. These findings align with previous results obtained using the same hull form [16]. Similar roughness effects have been observed in planning vessels [15].

References

[1] ITTC, "Specialist Committee on Surface Treatment," (26th International Towing Tank Conference, Newcastle University), 2 419- 481(2011).

[2] M. P. Schultz, "Frictional resistance of antifouling coating systems," J. Fluids Eng. Trans. ASME, 126:6, 1039-1047 (2004) doi: 10.1115/1.1845552.

[3] Y. K. Demirel, O. Turan and A. Incecik, Predicting the effect of biofouling on ship resistance using CFD, Appl. Ocean Res. 62 100-118(2017). doi: 10.1016/j.apor.2016.12.003.

[4] S. Song, Y. K. Demirel and M. Atlar, An investigation into the effect of biofouling on the ship hydrodynamic characteristics using CFD, Ocean Engineering 175 122–137(2019).

[5] J. Seok and J.-C. Park, Numerical simulation of resistance performance according to surface roughness in container ships, International Journal of Naval Architecture and Ocean Engineering 12 11–19(2020).

[6] T. Cebeci, Turbulence models and their application: efficient numerical methods with computer programs, European Journal of Mechanics - B/Fluids 24(3) 407 (2004) doi: 10.1016/j.euromechflu.2004.08.001.

[7] Z. Ali and G. Bognár, Investigation of the impact of surface roughness on a Ship's Drag (Hull Resistance), Acta Polytechnica Hungarica 21(2) 7-32 (2024).

[8] T. Hoch, " Development of a "numerical test bench" for turbine wheel gas meters," Diss. Duisburg, Essen, Universität Duisburg-Essen, Diss. 2011.

[9] CFD Online, "k-ω SST model," https://www.cfd-online.com/Wiki/SST_k-omega_model, August, 2013.

[10] F. R. Menter, M. Kuntz and R. Langtry, Ten years of industrial experience with the SST turbulence model, Turbulence, heat and mass transfer 4(1) 625-632(2003).

[11] "MOERI KVLCC2 Geometry and Conditions, SIMMAN 2008, FORCE Technology" http://www.simman2008.dk/KVLCC/KVLCC2/kvlcc2$_$geometry.html.

[12] IMO, 2012. Resolution MEPC.213(63) – 2012 Guidelines for the Development of a Ship Energy Efficiency Management Plan (SEEMP). International Maritime Organization, London, UK.

[13] IMO (2014). 2014 Guidelines on the Method of Calculation of the Attained Energy Efficiency Design Index (EEDI) for New Ships. Resolution MEPC.245(66), International Maritime Organization, London.

[14] IMO (2016). Guidelines for the Development of a Ship Energy Efficiency Management Plan (SEEMP). Resolution MEPC.282(70), International Maritime Organization, London.

[15] W. Amiruddin et al. "Prediction of the impact of biofouling roughness on a full-scale planing boat performance using CFD, Ocean Engineering 301 117457(2024).

[16] Z. Ali and G. Bognár, RANS study of surface roughness effects on ship resistance, Journal of Nonlinear, Complex and Data Science 25(2) 215-236(2024).

[17] R. Ravenna, S. Song, W. Shi, T. Sant, C.D.M. Muscat-Fenech, T.Tezdogan and Y.K. Demirel, CFD analysis of the effect of heterogeneous hull roughness on ship resistance, Ocean Engineering 258, 111733(2022).

[18] M.L. Hakim, A. Firdhaus, S. Samuel, S. Song, S. Kim and I.K.A.P. Utama, Investigating the impact of inhomogeneous roughness on the drag of a planing craft assisted by numerical simulation, Ocean Engineering 325, 120826(2025).

[19] R. Lopes, A. Eslamdoost, R. Johansson, S. RoyChoudhury, R.E. Bensow, P. Hogström and D. Ponkratov, Resistance prediction using CFD at model-and full-scale and comparison with measurements, Ocean Engineering 321, 120367(2025).

[20] C.G. Grlj, N. Degiuli, and I. Martić, I. Assessment of the effect of speed and scale on the total resistance and its components for a bulk carrier, Results in engineering, 105095(2025).

[21] W.S. Choi, G.S. Min, S.S. Han, H.C. Yun, M. Terziev, S. Dai and S. Song, Resistance and speed penalty of a naval ship with hull roughness, Ocean Engineering 312, 119058(2024).

[22] B. Pena and L. Huang, A review on the turbulence modelling strategy for ship hydrodynamic simulations, Ocean Engineering 241, 110082(2021).

[23] M. Zhu and L. Ma, A review of recent advances in the effects of surface and interface properties on marine propellers, Friction 12(2), 185-214(2024).

[24] Tanougast, A., & Hriczó, K. (2025). Comparison of Turbulence Models in the Simulation of Fluid Flow in Corrugated Channel. *Advances in Science and Technology*, *165*, 53-64.

[25] Tanougast, A., & Hriczó, K. (2025). Enhanced heat transfer in wavy channels with vortex generators: A CFD investigation. *International Journal of Thermofluids*, *30*, 101405.

[26] Perry, A. E., Schofield, W. H., & Joubert, P. N. (1969). Rough wall turbulent boundary layers. *Journal of Fluid Mechanics*, *37*(2), 383-413.

[27] Ali, Z., & Bognár, G. (2025). CFD-based analysis of ship resistance: Assessing the impact of surface roughness. *AIP Conference Proceedings, 3315(1),* 180001.

[28] Roache, P. J. (1998). *Verification and validation. Science and Engineering*. Hermosa Publ. Socorro New Mexico, USA.

[29] Esperança, M. N., Béttega, R., & Badino, A. C. (2017). Hydrodynamic evaluation of a square cross-section split airlift using CFD. *XXI Simpósio Nacional de Bioprocessos, XII Simpósio de Hidrólise Enzimática de Biomassa, Aracaju, Sergipe, Brasil.*